Pramana – J. Phys. (2017) 89:37
DOI 10.1007/s12043-017-1436-6

Graphene-based tunable terahertz filter with rectangular ring resonator containing double narrow gaps

WEI SU* and BINGYAN CHEN

Department of Mathematics and Physics, Hohai University, Changzhou Campus, Changzhou 213022, China
*Corresponding author. E-mail: opticSu@hotmail.com

MS received 14 October 2016; revised 19 March 2017; accepted 6 April 2017; published online 16 August 2017

Abstract. A plasmonic band-pass filter based on graphene rectangular ring resonator with double narrow gaps is proposed and numerically investigated by finite-difference time-domain (FDTD) simulations. For the filter with or without gaps, the resonant frequencies can be effectively adjusted by changing the width of the graphene nanoribbon, the coupling distance and chemical potential of graphene. In addition, by introducing narrow gaps in the rectangular ring resonators, it shows the single frequency filtering effect. Moreover, the structure also shows high sensitivity for different surrounding mediums. This work provides a novel method for designing all-optical integrated components in optical communication.

Keywords. Graphene surface plasmons; rectangular ring resonator; filter.

PACS Nos 42.25.Bs; 73.20.Mf; 78.20.Bh

1. Introduction

Surface plasmons (SPs) are coherent delocalized electron oscillations that exist at the metal–dielectric interface [1]. Recently, both theoretical and experimental studies have shown that surface plasmon polaritons (SPPs) can also propagate along the graphene surface [2–4]. Compared to the traditional noble metals, graphene has lots of advantages [5–10]. First, the thickness of the graphene layer is only one atomic scale, which is less than any metallic film. Secondly, graphene can support graphene surface plasmons (GSPs) from mid-infrared to terahertz frequencies, which can broaden the application of SPPs at these wave bands. Due to its high tunability and confinement, and low losses, GSPs have been investigated on many kinds of devices, such as optical switches [11], modulators [12], optical splitters [13], and so on.

Currently, many types of optical devices based on graphene have been investigated. Most of the devices are based on graphene nanoribbon (GNR), which can support both edge mode and waveguide mode [3,14]. If the width of the GNR is a few tens of nanometers, there will be only the edge mode. Due to the existence of the edge mode, GNR can realize great filtering effect, which is one of the most meaningful GSP applications. Moreover, by using graphene, the property of the filters can be tuned flexibly, and the size of the filters can be much smaller than that of the traditional optical filters.

In this paper, an ultracompact plasmonic filter based on graphene rectangular ring resonator with double narrow gaps is proposed. The transmission spectra and the electric field distribution in the filter are obtained by using the three-dimensional (3D) finite-difference time-domain (FDTD) method with perfect matching layer (PML) absorbing boundary conditions. For the filter structure with or without gaps, we investigate both the effects of structural parameters and chemical potential of graphene on transmission spectra. By changing the width of GNRs, the working frequency range and the transmission peak frequency can be changed. The band width of the filter can be tuned by changing different coupling distances between the lateral waveguide and the rectangular ring resonator. Besides, the resonant frequencies can be easily manipulated by appropriately changing the chemical potential of graphene, which enables us to obtain an electrically tunable pass-band filter without changing the structural parameters. Furthermore, the structure is highly sensitive to different surrounding mediums, showing its potential to be a biosensor. Our proposed structure can decrease the dimensions of the plasmonic filter and so can be used to design plasmonic integrated circuits.

2. Models and discussion

Figure 1 shows the schematic diagram of the proposed filter, which is composed of incoming and outgoing waveguides as well as a rectangular ring resonator with double narrow gaps. w is the width of the nanoribbon, l is the width of the rectangular ring resonator, d is the coupling length between the lateral waveguide and the resonator, g is the gap width. As shown in the inset, the graphene layer is deposited on the SiO_2/Si substrate. At mid-infrared frequency, the interband transition is suppressed. So the complex surface conductivity of graphene can be calculated from the simplified Kubo formula [2]:

$$\sigma_g = \frac{-ie^2 k_B T}{\pi\hbar^2(\omega - i2\Gamma)}\left(\frac{\mu_c}{k_B T} + 2\ln\left(e^{-\frac{\mu_c}{k_B T}} + 1\right)\right), \tag{1}$$

where e is the charge of the electron, k_B is the Boltzmann's constant, $\hbar = h/2\pi$ is the Planck's constant, ω is the radian frequency, μ_c is the chemical potential, Γ is the scattering rate and T is the temperature.

FDTD method with PML absorbing boundary condition is used to investigate the transmission property of the structure. Two power monitors are set at $Port_{in}$ and $Port_{out}$ to detect the input power P_{in} and the transmitted power P_{out}. So the transmissivity can be calculated as $T = P_{out}/P_{in}$.

First we consider the regular rectangular ring resonator filter without gaps [15]. A source is put at the left side to excite the fundamental edge mode in GNRs. Then, the GSP edge mode will be coupled into the rectangular ring resonator. Finally, the GSP wave that satisfies certain resonance conditions can be coupled to the exit port. Figure 2a shows the transmission spectra with different GNR widths, which proves the filtering property. The other parameters are set as $l = 120$ nm, $d = 10$ nm, $T = 300$ K and $\mu_c = 0.3$ eV. When the GNR width is 15 nm, it can be seen that there are three peaks corresponding to the frequencies of 9.97, 18.44 and 23.92 THz. When the GNR widths are 20 and 25 nm, there are peaks corresponding to the frequencies of 11.35, 20.99 THz and 12.66, 23.57 THz, respectively. The transmission peaks are 0.34, 0.63 and 0.53 at $w = 15$ nm, 0.44 and 0.78 at $w = 20$ nm and 0.68

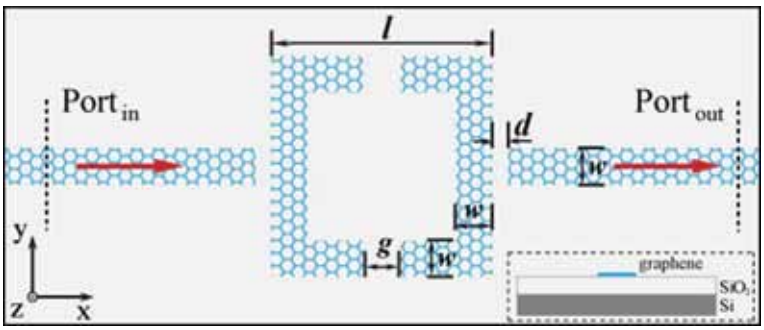

Figure 1. Schematic diagram of the rectangular ring resonator filter with double slits. w is the width of the nanoribbon, l is the width of the rectangular ring resonator, d is the coupling length between the lateral waveguide and the resonator, g is the gap width. The inset is the side view of the proposed filter with a graphene nanoribbon deposited on the SiO_2/Si substrate.

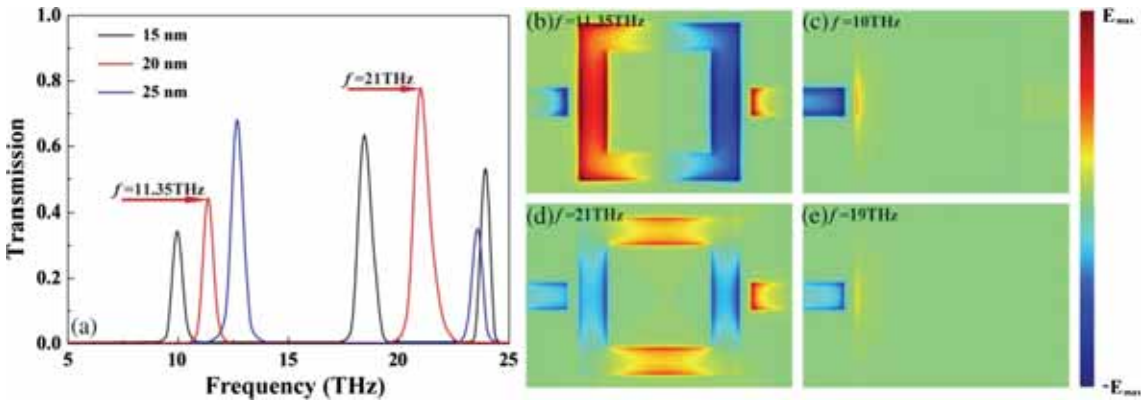

Figure 2. (**a**) The transmission spectra of the filter when nanoribbon width $w = 15$, 20 and 25 nm. The other parameters are set as $l = 120$ nm, $d = 10$ nm and $\mu_c = 0.3$ eV. (**b–e**) E_z field distribution in the structure at frequencies $f = 11.35$, 10, 21, 19 THz.

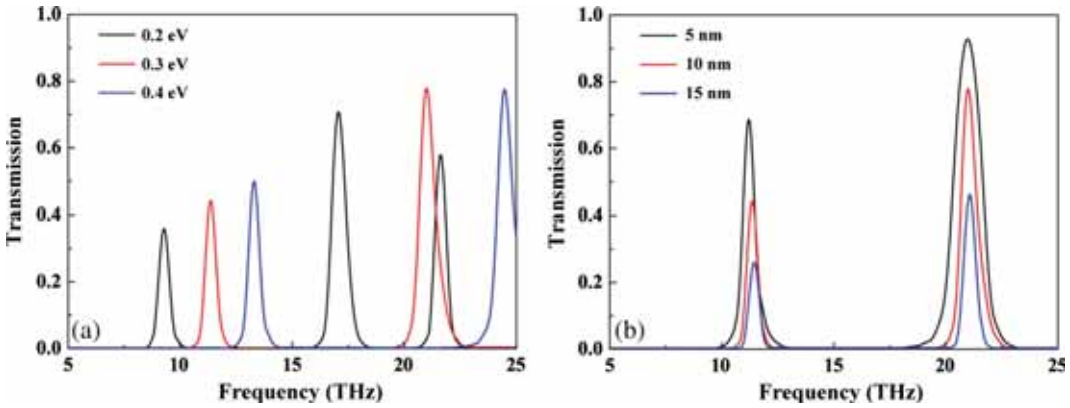

Figure 3. (**a**) The transmission spectra of the filter when chemical potential $\mu_c = 0.2$, 0.3 and 0.4 eV. The other parameters are set as $w = 20$ nm, $l = 120$ nm and $d = 10$ nm. (**b**) The transmission spectra of the filter with coupling distances $d = 5$, 10 and 15 nm. The chemical potential $\mu_c = 0.3$ eV.

and 0.35 at $w = 25$ nm. When the GNR width is 20 nm, the field profiles of the first- and second-order peaks are shown in figures 2b and 2d. When standing wave modes form in the resonator, most part of the GSPs can propagate through it and transmit into the exit port. Furthermore, the E_z field distribution of two transmission dips corresponding to the frequencies 10 and 19 THz are depicted in figures 2c and 2e, respectively. It shows that there is no excitation of the resonant cavity mode, the field in the rectangular resonator is very weak and the waves cannot pass through the filter.

Figure 3a shows transmission spectra of the GSPs for the structure for different chemical potentials μ_c. When chemical potential is 0.2 eV, there are three peaks corresponding to the frequencies of 9.28, 17.06 and 21.62 THz. When the chemical potentials are 0.3 and 0.4 eV, there are two peaks corresponding to the frequencies of 11.35, 20.99 THz and 13.30, 24.47 THz. The transmission peaks are 0.36, 0.71 and 0.58 at $\mu_c = 0.2$ eV, 0.44 and 0.78 at $\mu_c = 0.3$ eV and 0.50 and 0.77 at $\mu_c = 0.4$ eV. The resonant frequencies can be easily manipulated by changing the chemical potential of graphene.

For transmission calculation, the coupling distance d is also a very significant parameter affecting the transmission efficiency at the resonant modes. As shown in figure 3b, the transmission peaks at the coupling distance $d = 5$ nm are 0.68 and 0.93 at the first- and second-order peaks, 0.44 and 0.78 at $d = 10$ nm and 0.26 and 0.46 at $d = 15$ nm. The peak values decrease with increasing coupling distance d, because larger coupling distance can cause more energy coupled out of GNR. In addition, we can see that the resonant frequencies have a redshift by decreasing the coupling distance d, which is due to the changes of the phase shifts reflected on the two facets of the resonant GNR as the coupling distance changes [16].

Then we introduce double gaps with the width $g = 20$ nm in the middle of the rectangular ring resonator. Figure 4a shows the transmission spectra of the GSPs for the structure with different GNR widths from 15 to 25 nm. The other parameters are set as $l = 120$ nm, $d = 10$ nm, $T = 300$ K and $\mu_c = 0.3$ eV. Unlike the regular structure, it can be seen that there is only one peak for each GNR width, which shows the single frequency filtering effect. The resonant frequencies are 18.87, 21.49 and 23.89 THz corresponding to the GNR widths of 15, 20 and 25 nm, respectively, and the transmission peaks are 0.54, 0.82 and 0.24, respectively. When the GNR width w is 20 nm, the transmission peak reaches the maximum value. The E_z field profile of the peak for $w = 20$ nm is shown in figure 4b. It shows that most of the GSPs can propagate through the filter. In addition, the E_z field distribution corresponding to 19 THz frequency is depicted in figure 4c. It shows that the GSPs cannot pass through the filter.

Figure 5a gives the transmission spectra for different coupling distances d. There is only one peak for each coupling distance. As in figure 3b, the peak values decrease with increase in coupling distance d. We can also see that the resonant frequencies have a redshift by decreasing the coupling distance d. Figure 5b shows the transmission spectra of the filter with different gap widths. It is obvious that the resonant frequencies increase as g increases. We also find that the transmission peaks have a nonlinear relationship with g. When the gap width is 20 nm, the transmission peak reaches the maximum value 0.82.

Figure 6a shows the transmission spectra of the GSPs for the structure with different chemical potentials μ_c. There is only one peak for each chemical potential as well. The resonant frequencies are 17.37, 21.49 and 24.85 THz corresponding to the chemical potentials 0.2, 0.3 and 0.4 eV, respectively, and the transmission peaks

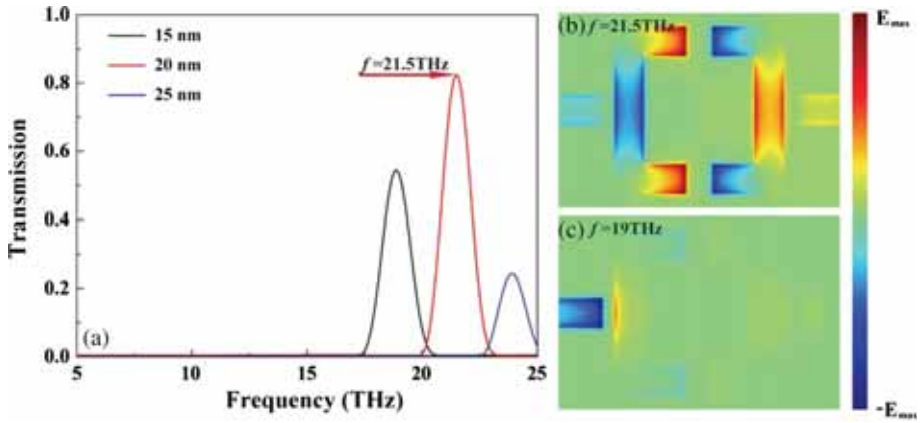

Figure 4. (**a**) The transmission spectra of the filter when nanoribbon width $w = 15$, 20 and 25 nm. The other parameters are set as $l = 120$ nm, $d = 10$ nm, $g = 20$ nm and $\mu_c = 0.3$ eV. (**b, c**) E_z field distribution in the structure at frequency $f = 21.5$ and 19 THz, respectively.

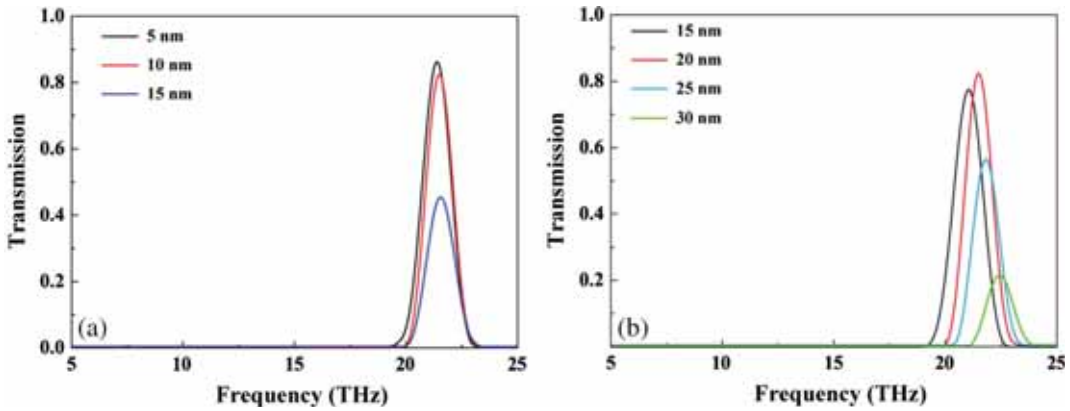

Figure 5. (**a**) The transmission spectra of the filter when coupling distance $d = 5$, 10 and 15 nm. The other parameters are set as $w = 20$ nm, $l = 120$ nm, $g = 20$ nm and $\mu_c = 0.3$ eV. (**b**) The transmission spectra of the filter when gap width $g = 15$, 20, 25 and 30 nm. The other parameters are set as $w = 20$ nm, $l = 120$ nm, $d = 10$ nm and $\mu_c = 0.3$ eV.

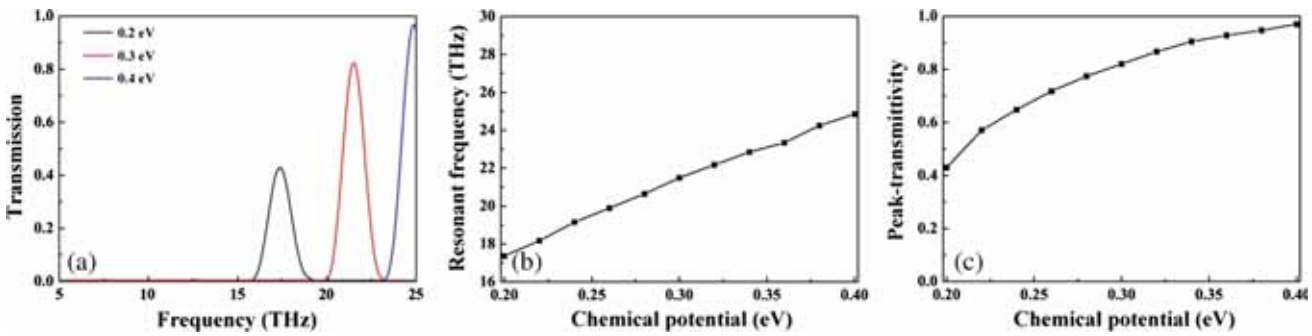

Figure 6. (**a**) The transmission spectra of the filter when the chemical potential $\mu_c = 0.2$, 0.3 and 0.4 eV. The other parameters are set as $w = 20$ nm, $l = 120$ nm, $g = 20$ nm and $d = 10$ nm. (**b**) The resonant frequency as a function of chemical potential. (**c**) The peak transmittivity as a function of chemical potential.

are 0.43, 0.82 and 0.97, respectively. Figure 6b shows the resonant frequency as a function of chemical potential. The frequency range is from 17.37 to 24.85 THz. So the pass-band centre frequency can be tuned easily by changing chemical potential without changing the dimensions of the filter, which offers greater flexibility and performance than conventional metallic plasmonic devices. As shown in figure 6c, the transmission peaks

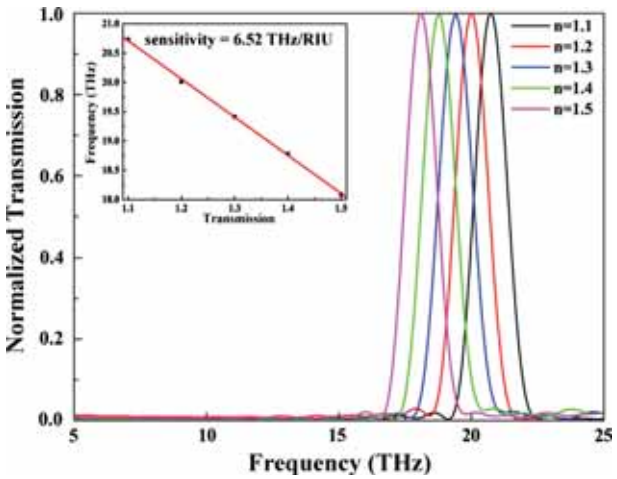

Figure 7. The transmission spectra of the filter with different refractive indices of the surrounding mediums. The refractive index varies from 1.31 to 1.35. The inset shows the linear regression analysis between resonant frequency and refractive index of the surrounding mediums.

increase with the increase of the chemical potential. It is due to fact that as the chemical potentials decrease, the dissipation losses will increase, leading to the decrease of the energy transmitted in the exit port [9].

At last, we consider the relationship between the peak location and the nearby dielectric medium. Figure 7 shows the normalized transmission spectra with different refractive indices of the surrounding mediums. The structural parameters are not changed. From the curves, it can be observed that the peaks move to the left gradually as the refractive index increases. The inset shows the linear regression analysis between resonant frequency and refractive index of the surrounding medium. The sensitivity is 6.52 THz/RIU, which is much larger than that in [17,18]. This high sensitivity makes the filter a good plasmonic biosensor.

3. Conclusions

In this paper, a compact plasmonic filter based on graphene rectangular ring resonator with double narrow gaps has been proposed. For the filter, with or without gaps, simulation results based on FDTD method show that the transmission spectra can be affected by the width of the graphene nanoribbon, the coupling distance between the lateral waveguide and the rectangular ring resonator and the chemical potential of graphene. Furthermore, the structure also shows high sensitivity with refractive indices of the surrounding mediums. The fabrication of our structure is simple and it can decrease plasmonic filter dimensions, based on which we shall find potential applications in highly integrated optical circuits.

Acknowledgements

This work is partially supported by the NSFC (Grant Number 11274092), the Fundamental Research Fund for Central Universities of China (Grant Number 2016B12314, 2015B27914), and the Open Project of Jiangsu Province Key Laboratory of Environmental Engineering (Grant Number KF2014001). The authors would especially like to thank Dr Yun Da from Nanjing University of Science and Technology for his helpful discussions and the use of FDTD Solutions.

References

[1] W L Barnes, A Dereux and T W Ebbesen, *Nature* **424**, 824 (2004)
[2] G W Hanson, *J. Appl. Phys.* **103**, 064302 (2008)
[3] A Y Nikitin, F Guinea, F J García-Vidal and L Martín-Moreno, *Phys. Rev. B* **84**, 161407 (2011)
[4] M Jablan, H Buljan and M Soljačić, *Phys. Rev. B* **80**, 245435 (2009)
[5] T B Wang, X W Wen, C P Yin and H Z Wang, *Opt. Express* **17**, 24096 (2009)
[6] L Ju, B Geng, J Horng, C Girit, M Martin, Z Hao, H A Bechtel, X Liang, A Zettl, Y R Shen and F Wang, *Nat. Nanotechnol.* **6**, 630 (2011)
[7] A Vakil and N Engheta, *Science* **332**, 1291 (2011)
[8] T Low and P Avouris, *ACS Nano* **8**, 1086 (2014)
[9] H W Zhuang, F M Kong, K Li and S W Sheng, *Appl. Opt.* **54**, 2558 (2015)
[10] G G Zheng, L H Xu and Y Z Liu, *Pramana – J. Phys.* **86**, 1091 (2016)
[11] J S Gómez-Díaz and J Perruisseau-Carrier, *Opt. Express* **21**, 15490 (2013)
[12] B Sensale-Rodriguez, R Yan, M Zhu, D Jena, L Liu and H G Xing, *Appl. Phys. Lett.* **101**, 261115 (2012)
[13] X Zhu, W Yan, N A Mortensen and S Xiao, *Opt. Express* **21**, 3486 (2013)
[14] S He, X Zhang and Y He, *Opt. Express* **21**, 30664 (2013)
[15] A Setayesh, S R Mirnaziry and M S Abrishamian, *J. Opt.* **13**, 035004 (2011)
[16] F Ma and X Liu, *Appl. Opt.* **46**, 6247 (2007)
[17] B F Yun, G H Hu, J W Cong and Y P Cui, *Plasmonics* **9**, 691 (2014)
[18] G L Fu, X Zhai, H J Li, S X Xia and L L Wang, *Plasmonics* **11**, 1597 (2016)